Available online at www.sciencedirect.com
ScienceDirect
Journal of Sound and Vibration 311 (2008) 184–199
JOURNAL OF SOUND AND VIBRATION
www.elsevier.com/locate/jsvi

# The influence of shape and material anisotropy on the vibrational modes of free particles

P.R. Heyliger[a,*], E. Pan[b], S. Cook[a], Marlo Manaloto[c]

[a]Department of Civil Engineering, Colorado State University, Fort Collins, CO 80523-1372, USA
[b]Department of Civil Engineering, University of Akron, Akron, OH 44325-3905, USA
[c]Rose-Hulman Institute of Technology, Terre Haute, IN 47803, USA

Received 10 January 2006; received in revised form 22 August 2007; accepted 29 August 2007
Available online 10 October 2007

**Abstract**

The influence of specimen geometry and material anisotropy on the vibrational modes of free-standing particles is investigated using a variational method applied to the traction-free vibration of elastic solids. The geometric shapes of spheres, cubes, and pyramids with both isotropic and cubic material symmetry are explored for a variety of compounds. It is shown that the shape and inclusion of anisotropy in the elastic stiffness tensor are both critical parameters in the frequency spectra, and that these features must be modeled for an accurate representation of both free and embedded particles.
© 2007 Elsevier Ltd. All rights reserved.

## 1. Introduction

The problem of traction-free vibration of elastic solids has become a hugely important area of study with numerous applications ranging from non-destructive evaluation to the evaluation of material properties. In nearly all applications, an accurate representation of both the geometry of the solid and the level of material anisotropy is of significant interest in that it is not uncommon to assume isotropic behavior for an anisotropic material or use an assumed shape of a sphere for an irregular non-spherical particle.

A typical example where these assumptions are often invoked are quantum nanostructures, which show certain unique features due to their electronic energy confinements in different directions, and thus can be applied to a variety of semiconductor devices [1–3] or more generic studies of particles whose characteristic dimensions are at the nanoscale [4–12]. Many recent studies on the induced strain fields in these structures, based either on molecular-dynamics or continuum methods, have clearly indicated the importance of the material anisotropy on the induced fields. Nearly all of the models used in previous dynamic studies are based on the assumption that the particles are elastically isotropic and are of spherical shape.

Another class of problem in which the assumption of material isotropy and spherical particle shape are frequently assumed is the field of particle compaction [13,14]. The reasons for using these assumptions are

*Corresponding author.
*E-mail addresses:* prh@engr.colostate.edu (P.R. Heyliger), Pan2@uakron.edu (E. Pan).

0022-460X/$ - see front matter © 2007 Elsevier Ltd. All rights reserved.
doi:10.1016/j.jsv.2007.08.036

usually to allow for a much simpler form of analysis, particularly using discrete element methods [15–18]. This is in contrast to alternative representations of the particle, such as that given in the present study, in which power series representations of the fields are used over the specific domain of a particle that can be spherical or otherwise [19]. In the case of particle vibration, the solution for an isotropic sphere can be obtained in closed form rather than the far more complex problem of an anisotropic particle of non-spherical shape. In particle compaction, the assumption of spherical particles allows for much simpler contact algorithms using local deformation laws. However, the actual influence of particle shape and anisotropy in aggregate particle compaction remains an area of current study that could be influenced by the results of the individual particle mechanics as represented in this work.

The intent of the present study is to examine the effect of anisotropy and shape on the vibrational modes of free particles, and therefore to estimate the levels of error that are induced by invoking the simplifying assumptions of either spherical shape or material isotropy. To solve this problem, we apply a variational method to the unrestrained free vibration of elastic solids. This approach uses the fundamentals of continuum mechanics, and hence any limitations in continuum theory as the particles approach the nanoscale will not be explored in this work. The particles are modeled as spheres, cubes, and pyramids for a variety of compounds with both isotropic and cubic symmetry. This latter geometry is important, as results for this shape have not yet appeared in the literature but they can in fact appear as quantum dot nanostructures [3]. It is expected that this geometry will have numerous future applications. It is shown that both the shape and elastic anisotropy of the particles can have significant influence on the vibrational spectra, and thus these features must be modeled for an accurate representation of both free-standing and embedded particles.

## 2. Problem description and governing equations

### 2.1. Equations of motion and weak form

The particles are assumed to consist of linear elastic solids with constitutive equations expressed in Cartesian coordinates as [20]

$$\sigma_{ij} = C_{ijkl}\varepsilon_{kl}, \tag{1}$$

where $\sigma_{ij}$, $C_{ikjl}$, and $\varepsilon_{ij}$ are the components of stress, the elastic stiffness tensor, and the infinitesimal strain tensor, respectively. In matrix form, the elements of the tensor $\boldsymbol{C}$ (with components $C_{ijkl}$) for a generic orthotropic solid can be expressed as

$$[C] = \begin{bmatrix} C_{11} & C_{12} & C_{13} & 0 & 0 & 0 \\ & C_{22} & C_{23} & 0 & 0 & 0 \\ & & C_{33} & 0 & 0 & 0 \\ & & & C_{44} & 0 & 0 \\ & Sym & & & C_{55} & 0 \\ & & & & & C_{66} \end{bmatrix}. \tag{2}$$

If the constitutive relation is expressed in this matrix form, the conventional contracted notation ($\sigma_{11} = \sigma_1$, $\sigma_{23} = \sigma_4$, $\varepsilon_{11} = \varepsilon_1$, $2\varepsilon_{23} = \varepsilon_4$, $C_{1111} = C_{11}$, $C_{1123} = C_{14}$, and so on) is assumed, and it is understood that the 1, 2, 3 directions are $x_1 = x$, $x_2 = y$, and $x_3 = z$.

The general strain–displacement relation is given by

$$\varepsilon_{ij} = 0.5(u_{i,j} + u_{j,i}), \tag{3}$$

where $u_i$ ($i = 1,2,3$) represent the components of elastic displacement within the particle. Substitution of the constitutive relations and strain–displacement relations into the equations of motion

$$\sigma_{ij,j} = \rho \frac{\partial^2 u_i}{\partial t^2} \tag{4}$$

yields three differential equations of motion in the three displacement variables $(u_1,u_2,u_3)$. To determine the acoustic modes of free-standing particles, the tractions on the boundary surfaces of the solid are specified to be zero. There are no specified displacements for this class of boundary-value problem, and hence there will be six rigid-body modes corresponding to a frequency of zero.

Exact solutions for most solid objects are, with some important exceptions, very difficult to obtain. The general approach used in this study is the Ritz method applied to the problem of unrestrained free vibrations. Hamilton's principle for an elastic medium is the starting point for such an analysis, and is given by [20]

$$\delta \int_{to}^{t} \mathrm{d}t \int_V [\tfrac{1}{2}\rho \dot{u}_j \dot{u}_j - \tfrac{1}{2} C_{ijkl}\varepsilon_{ij}\varepsilon_{kl}]\,\mathrm{d}V + \int_{to}^{t} \mathrm{d}t \int_S \bar{t}_k \delta u_k \,\mathrm{d}S = 0. \tag{5}$$

Here $t$ denotes time, $V$ and $S$ the volume and surface occupied by and bounding the solid, $\bar{t}_k$ the components of the specified surface tractions, $\delta$ the variational operator, and the overdot denotes the differentiation with respect to time. For the free-standing particle, the specified tractions on the surfaces of the solid are zero, and the surface integral will vanish. In contracted notation, this relationship becomes

$$\begin{aligned} 0 = & -\int_0^t \int_V \{\sigma_1\delta\varepsilon_1 + \sigma_2\delta\varepsilon_2 + \sigma_3\delta\varepsilon_3 + \sigma_4\delta\varepsilon_4 + \sigma_5\delta\varepsilon_5 + \sigma_6\delta\varepsilon_6\}\,\mathrm{d}V\,\mathrm{d}t \\ & + \frac{1}{2}\delta \int_0^t \int_V \rho(\dot{u}^2 + \dot{v}^2 + \dot{w}^2)\,\mathrm{d}V\,\mathrm{d}t. \end{aligned} \tag{6}$$

Using the assumptions of periodic motion and inserting the constitutive relations of Eq. (1) and the strain–displacement relations of Eq. (3) yields the final weak form of the equations of motion. It is this expression for which approximate solutions must be sought for problems with no exact solution.

### 2.2. The sphere: exact solutions

The torsional modes of an isotropic, elastic sphere can be found exactly by solving the characteristic equations of motion (4) for the frequency parameter $\eta$, given as

$$\frac{\mathrm{d}}{\mathrm{d}\eta}\left(\frac{j_l(\eta)}{\eta}\right) = 0, \tag{7}$$

where $j_l$ is the spherical Bessel function of order l. The torsional modes of an isotropic sphere are somewhat unusual in that they do not depend on the elastic constants of the material, but only on the geometry. Spheroidal modes are characterized by deformations resulting in dilatation, and are found using solutions of the characteristic equation

$$\begin{aligned} & 2\left\{\eta^2 + (l-1)(l+2)\left[\frac{\eta j_{l+1}(\eta)}{j_l(\eta)} - (l+1)\right]\right\}\frac{\zeta j_{l+1}(\zeta)}{j_l(\zeta)} - \frac{\eta^4}{2} + (l-1)(2l+1)\eta^2 \\ & \quad + [\eta^2 - 2l(l-1)(l+2)]\frac{\eta j_{l+1}(\eta)}{j_l(\eta)} = 0. \end{aligned} \tag{8}$$

For given values of l, the $n$th frequency can be calculated from solution of this equation. This very important result was first obtained by Lamb in 1882 [21] and the resulting characteristics of the motion were later expanded in some detail in a sequence of papers by Sato and Usami [22,23]. These results are significant in part because they provide one of the very few exact mathematical results for unrestrained free-vibration of elastic solids, and is one of the dominant reasons why the model of nanostructures as isotropic spheres has been so prevalent in the literature. The resulting frequencies from these calculations will be used later in this study to confirm the numerical procedure used in this study and to provide baseline numerical results for isotropic spheres.

### 2.3. The general anisotropic solid: the approximate model

For the general anisotropic solid, it is not possible to obtain an exact solution to the free vibration problem. The Ritz method provides an alternative means of computing the frequencies of elastic solids when either the material is anisotropic or the solid is not of spherical shape. This method has been used extensively to study the resonant modes of anisotropic solids, such as the work of Visscher et al. [24] and Heyliger and Jilani [25]. Using power series as the basis functions for this approach allows for both exact and simple integration of the integrals implied by Eq. (6) and also allows for separation of the frequencies into specific modal groups [24]. The approximations for the three displacement components can be written in this case as

$$u(x,y,z) = \sum_{j=1}^{m} a_j \Psi_j^u(x,y,z), \tag{9a}$$

$$v(x,y,z) = \sum_{j=1}^{n} b_j \Psi_j^v(x,y,z), \tag{9b}$$

$$w(x,y,z) = \sum_{j=1}^{p} d_j \Psi_j^w(x,y,z). \tag{9c}$$

Here $a$, $b$, and $d$ are constants associated with the $j$th approximation function for $u$, $v$, and $w$, respectively, the $\Psi$ functions are the approximation functions for each of the three variables, and $m$, $n$, and $p$ are the number of terms selected for each of the three series approximations. In this study, the approximation functions are selected as power series in $x$, $y$, and $z$ (e.g. 1, $x$, $y$, $z$, $xy$, $xz$, $yz$, $xyz$, $x^2$, and so on). Substitution of these approximations into the weak form of Eq. (6) results in a standard generalized eigenvalue problem that can be solved using standard techniques. This methodology has been discussed elsewhere [24,25] and will not be repeated here.

The use of power series in Cartesian coordinates regardless of geometric shape allows a grouping of the approximation functions in such a way as to reduce the size of the resulting eigenvalue problem. Depending on the shape used to model the particle and the type of material symmetry assumed, this grouping can significantly reduce computational effort. For example, the modes for the isotropic sphere as formulated in Cartesian coordinates can be split into eight separate modal groups, while the modes for a pyramid composed of a material with cubic symmetry can be split into four groups. For other geometries and material symmetries, different groupings are possible [26–28], and we note only that this approach was exploited to the maximum possible effect in all of the numerical results that follow.

## 3. Numerical results

This section contains two separate discussions. First, the relative accuracy of the computational method is briefly discussed. We then apply this methodology to a wide array of particle geometries with varying material properties.

### 3.1. Accuracy of the method

Before considering the comparisons of most interest in this study, it is useful to comment on the relative accuracy of the present method. Below we briefly discuss the relative accuracy of this method when applied to spheres, parallelepipeds, and pyramids with isotropic material symmetry.

#### 3.1.1. The sphere

The Ritz model as applied in this study does not allow simple classification of spheroidal or torsional modes as is the case when the problem is solved in spherical coordinates. Yet even without this benefit, the accuracy of this approach is excellent. An example is shown in Table 1, which shows the convergence of frequencies of

Table 1
Convergence of frequencies for the isotropic sphere using the present Ritz method

| $\lambda = 6$ | $\lambda = 8$ | $\lambda = 10$ | $\lambda = 12$ | Exact | Mode |
|---|---|---|---|---|---|
| 2.501 (5) | 2.501 | 2.501 | 2.501 | 2.501 | $T(1,1)$ |
| 2.640 (5) | 2.64 | 2.64 | 2.64 | 2.64 | $S(2,1)$ |
| 3.425 (3) | 3.425 | 3.425 | 3.424 | 3.424 | $S(1,2)$ |
| 3.868 (7) | 3.865 | 3.865 | 3.865 | 3.865 | $T(2,1)$ |
| 3.917 (7) | 3.916 | 3.916 | 3.916 | 3.916 | $S(3,1)$ |
| 4.440 (1) | 4.44 | 4.44 | 4.44 | 4.44 | $S(0,1)$ |
| 4.883 (5) | 4.865 | 4.865 | 4.865 | 4.865 | $S(2,2)$ |
| 5.105 (9) | 5.011 | 5.009 | 5.009 | 5.009 | $S(4,1)$ |
| 5.139 (9) | 5.095 | 5.095 | 5.095 | 5.095 | $T(4,1)$ |
| 5.856 (3) | 5.765 | 5.763 | 5.763 | 5.763 | $T(1,2)$ |
| 6.247 (11) | 6.036 | 6.033 | 6.033 | 6.033 | $S(5,1)$ |
| 6.504 (7) | 6.287 (11) | 6.266 | 6.266 | 6.266 | $T(5,1)$ |
| 6.814 (3) | 6.456 (7) | 6.454 | 6.454 | 6.454 | $S(3,2)$ |
| 7.211 (11) | 6.773 (3) | 6.772 | 6.771 | 6.771 | $S(1,3)$ |
| 7.330 (5) | 7.143 (13) | 7.029 | 7.023 | 7.023 | $S(6,1)$ |
| 7.998 (3) | 7.238 (5) | 7.136 | 7.136 | 7.136 | $T(2,2)$ |
| 8.660 (13) | 7.44 (13) | 7.404 | 7.404 | 7.404 | $T(6,1)$ |
| 9.307 (5) | 7.76 (3) | 7.747 | 7.745 | 7.744 | $T(3,2)$ |
| 9.554 (9) | 8.173 (9) | 8.004 (15) | 7.995 | 7.995 | $S(7,1)$ |
| 10.743 (1) | 8.396 (15) | 8.066 (9) | 8.061 | 8.062 | $S(4,2)$ |
| 11.402 (13) | 8.518 (5) | 8.338 (5) | 8.322 | 8.329 | $S(2,3)$ |
| 11.436 (7) | 8.772 (7) | 8.462 (7) | 8.442 | 8.444 | $T(3,2)$ |
| 11.565 (11) | 9.729 (3) | 8.575 (15) | 8.521 | 8.52 | $T(7,1)$ |
| 13.116 (7) | 9.848 (11) | 9.140 (3) | 8.968 | 8.955 | $S(8,1)$ |
| 13.416 (12) | 10.066 (4) | 9.454 (6) | 9.065 | 9.095 | $T(1,3)$ |

The number in parentheses indicates the number of degenerate modes at that specific frequency. As more terms are used, there can be shifts in frequency, and hence this number can be updated with the final and more accurate value in a column on the right. The column in the far right indicates the modal group type using the nomenclature of Sato and Usami [22], with $T$ and $S$ denoting torsional and spheroidal modes, respectively.

an isotropic sphere when compared with the analytic solution solved in terms of Bessel functions as originally computed by Lamb [21]. We use the parameter $\lambda$ as the convergence variable both for this example and the rest of this study, where this symbol denotes the sum of the individual powers in $x$, $y$, and $z$ (i.e. if the approximation functions are expressed as $x^q y^r z^s$, then series up to and including $\lambda = q+r+s$ are used in the series approximation for each of the variables). Frequencies computed using $\lambda = 10$ are in excellent agreement with the exact solution for the first 60 or so frequencies for the isotropic sphere. We use this accuracy to justify the use of $\lambda = 10$ in later calculations. Also of note is the extremely large number of degenerate frequencies for the isotropic sphere. These are denoted by the parenthetical number to the right of each frequency in Table 1. When the material is anisotropic or the solid not exactly spherical, the frequencies are not exactly the same but instead appear within a very tightly packed frequency range. When the material possesses cubic material symmetry, the number of degenerate frequencies drops significantly, as we show in a later section.

### 3.1.2. The parallelepiped

Another geometric shape that can be used to model typical nanoparticle geometries is that of the cube. In this case, the same formulation used for the sphere can be used again, with the domains of integration changed to model the change in geometry. This approach was originally used by Demarest [29] and has also seen extensive applications in numerous studies. We do not show representative results for this geometry, but note that the level of accuracy is similar to that of the sphere for $\lambda = 10$.

### 3.1.3. The pyramid

There are very few published studies on the acoustic modes or free vibration behavior of solid pyramids [30], although the use of the Ritz model as used here was first discussed by Visscher et al. [24] but with no numerical

results given. Use of power series as basis functions allows for computation of the frequencies and modal shapes of pyramids with base half-lengths of $d_1$ and $d_2$ and a height of $d_3$. This allows for exact computation of the volume integrals required by the variational model.

Since there are no results available for comparison, we test the accuracy and validity of our Ritz algorithm by comparing our results with those of a three-dimensional finite element solution to the equations of motion. We omit details of this formulation, as the variational formulation is identical to that given here for the solids under investigation and the element matrices are also the same. The only difference is in the nature of the approximation functions for the three displacement variables. In the Ritz model, these functions are global and span the entire domain of the solid. In a finite element model, these approximations are piecewise and span only over the domain of a typical finite element. In this representation, we use 8-noded brick elements. When there are pyramid shaped elements, we collapse the edges into the appropriately shaped element. The relative test pyramid dimensions are given as $d_1 = d_2 = d_3$. A total of four meshes are used to represent the pyramid to show the convergence characteristics. Mesh 1 has 35 nodes and 20 elements, mesh 2 has 69 nodes and 40 elements, mesh 3 has 165 nodes with 120 elements, and mesh 4 has 969 nodes with 816 elements. The resulting frequencies are shown in Table 2 and are compared with the frequencies from the Ritz model using $\lambda = 10$ terms in the approximation. The values shown in the table are the dimensionless frequencies $\varpi = \omega d_1/C_t$ where $\omega$ is the natural frequency and $C_t$ is the shear wave speed defined by $(C_{44}/\rho)^{1/2}$.

Table 2
The convergence of the first 30 modal frequencies of the isotropic pyramid is shown as a function of mesh size

| Mode | FEM | | | | Ritz |
|---|---|---|---|---|---|
| | Mesh 1 | Mesh 2 | Mesh 3 | Mesh 4 | |
| 1 | 1.8208 | 1.5872 | 1.5250 | 1.4546 | 1.4309 |
| 2 | 2.5026 | 2.1905 | 2.0931 | 1.9403 | 1.8856 |
| 3 | 2.5083 | 2.1905 | 2.1356 | 2.0102 | 1.9635 |
| 4 | 2.5083 | 2.2556 | 2.1356 | 2.0102 | 1.9635 |
| 5 | 2.6470 | 2.4605 | 2.3013 | 2.1620 | 2.1032 |
| 6 | 2.9299 | 2.7102 | 2.5596 | 2.3980 | 2.3237 |
| 7 | 3.0832 | 2.7102 | 2.5596 | 2.3980 | 2.3237 |
| 8 | 3.2100 | 2.7292 | 2.6061 | 2.4362 | 2.3850 |
| 9 | 3.2230 | 2.7594 | 2.6953 | 2.4755 | 2.4051 |
| 10 | 3.2230 | 2.9828 | 2.7383 | 2.4755 | 2.4051 |
| 11 | 3.4642 | 2.9828 | 2.7383 | 2.6344 | 2.6109 |
| 12 | 3.4642 | 2.9898 | 2.8980 | 2.8143 | 2.7845 |
| 13 | 3.7116 | 3.3365 | 3.1463 | 2.9972 | 2.9427 |
| 14 | 4.0067 | 3.4047 | 3.2059 | 3.0103 | 2.9493 |
| 15 | 4.0121 | 3.5613 | 3.3770 | 3.1599 | 3.0740 |
| 16 | 4.0121 | 3.5613 | 3.3770 | 3.1599 | 3.0740 |
| 17 | 4.4535 | 4.1010 | 3.9854 | 3.4577 | 3.2234 |
| 18 | 4.5853 | 4.3576 | 3.9854 | 3.4683 | 3.2234 |
| 19 | 4.5853 | 4.3576 | 4.0236 | 3.4683 | 3.2241 |
| 20 | 5.4007 | 4.5028 | 4.0455 | 3.5816 | 3.4181 |
| 21 | 5.5010 | 4.5203 | 4.0575 | 3.6932 | 3.4698 |
| 22 | 5.6903 | 4.6923 | 4.1454 | 3.8455 | 3.6959 |
| 23 | 5.8469 | 4.7261 | 4.2576 | 3.8682 | 3.7657 |
| 24 | 5.8469 | 4.7261 | 4.2806 | 3.8682 | 3.7657 |
| 25 | 5.9825 | 5.1142 | 4.2806 | 3.8810 | 3.8153 |
| 26 | 6.1302 | 5.2595 | 4.9636 | 4.2991 | 3.9957 |
| 27 | 6.1467 | 5.2595 | 4.9636 | 4.2991 | 3.9957 |
| 28 | 6.1467 | 5.4050 | 5.0147 | 4.6265 | 4.2955 |
| 29 | 6.1746 | 5.6431 | 5.0687 | 4.6265 | 4.4433 |
| 30 | 6.3816 | 5.7321 | 5.0687 | 4.6391 | 4.4433 |

The repeated frequencies appear from both structural and material symmetry.

This comparison is presented for two reasons. First, the authors are unaware of any previous results for free vibration response spectra for pyramids, and the finite element results are a useful means of comparison. The convergence trends appear to be very good, with the frequencies of the most refined mesh being within several percent of the Ritz results for most modes and no greater than five percent higher than the Ritz model for the higher frequencies. Both the finite element and Ritz methods converge from above, so the Ritz frequencies are the more accurate of the two. The second reason for this comparison is to show the level of accuracy of the present Ritz model compared to the more typically used finite element method. For the level of approximation

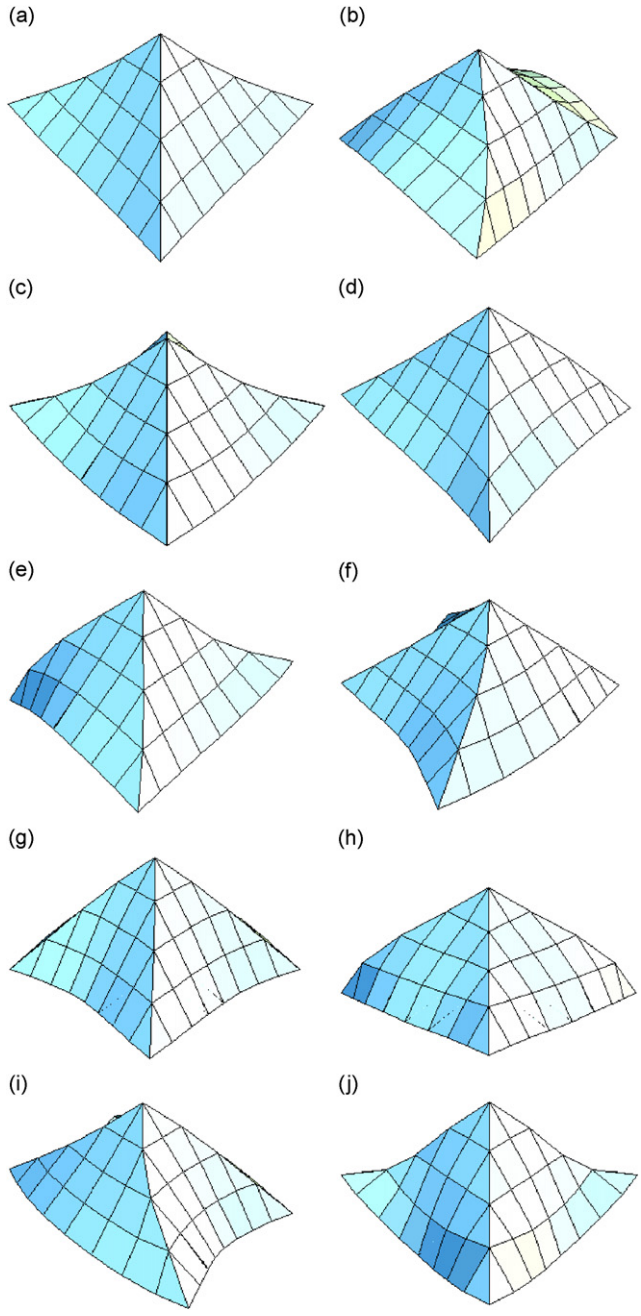


Fig. 1. The first ten modes of traction-free vibration for an isotropic pyramid. (a) Mode 1, (b) Mode 2, (c) Mode 3, (d) Mode 4, (e) Mode 5, (f) Mode 6, (g) Mode 7, (h) Mode 8, (i) Mode 9, (j) Mode 10.

used ($\lambda = 10$), the use of group theory allows the complete eigenvalue problem associated with functions of this order to be separated into four smaller eigenvalue problems of dimension 216, 195, 231, and 216. These numbers vary depending on the order of approximation, type of material symmetry, and shape of the solid. They are given here only as representative examples of the ordering reduction using symmetry of modal groups. The finest mesh used in this study uses over ten times the number of degrees of freedom than that of the Ritz model, but is still less accurate than when using global basis functions. It would be possible to exploit symmetry features of the vibrational modes to reduce the size of the finite element mesh, but even the use of this tactic does not result in higher accuracy per degree of freedom.

We also show the first ten independent modes of a free-standing pyramid in Fig. 1. These are plotted using the respective eigenvectors that correspond to the frequencies given in Table 2.

### 3.2. Geometry and material symmetry

In this section, we compute and compare the acoustic modes of free particles composed of a wide array of materials using assumed geometric shapes of spheres, parallelepipeds, and pyramids. The materials used in this study are Ge, Si, Ag, Au, GaSb, AlSb, GaN, AlN, and AlAs. The elastic constants for the first four of these crystals are taken from Hirth and Lothe [31] and those for the latter five are from Vurgaftman et al. [32] and are shown in Tables 3 and 4. Each of these crystals possess cubic material symmetry, and the level of material anisotropy for each crystal is denoted by the dimensionless parameter $A = |C_{11} - C_{12} - 2C_{44}|/C_{44}$. This parameter is zero when the material is isotropic, and increases with the level of anisotropy.

For each of the crystals considered, six separate analyses are completed. For specimens with the same total mass, the frequencies for unrestrained free vibration are computed first using the assumption of isotropic

Table 3
Elastic constants (in GPa) for various materials used in frequency calculations and the degree of anisotropy factor $A = |C_{11} - C_{12} - 2C_{44}|/C_{44}$

| Crystal | $C_{11}$ | $C_{12}$ | $C_{44}$ | $A$ |
|---|---|---|---|---|
| *Cubic elastic constants* | | | | |
| Ge | 128.9 | 48.3 | 67.1 | 0.80 |
| Si | 165.7 | 63.9 | 79.6 | 0.72 |
| Ag | 124.0 | 93.4 | 46.1 | 1.34 |
| Au | 186.0 | 157.0 | 42.0 | 1.31 |
| GaSb | 884.2 | 402.6 | 432.2 | 0.89 |
| AlSb | 876.9 | 434.1 | 407.6 | 0.91 |
| GaN | 293 | 159 | 155 | 1.14 |
| AlN | 304 | 160 | 193 | 1.25 |
| AlAs | 1250 | 534 | 542 | 0.68 |

Table 4
Isotropic polycrystalline elastic constants from averaged monocrystal elastic constants (in GPa)

| Crystal | $C_{11}$ | $C_{44}$ | $\upsilon$ |
|---|---|---|---|
| Ge | 148.2 | 54.76 | 0.2069 |
| Si | 186.6 | 66.60 | 0.2226 |
| Ag | 143.9 | 30.20 | 0.3671 |
| Au | 204.1 | 28.06 | 0.4203 |
| GaSb | 1019.9 | 342.6 | 0.2471 |
| AlSb | 1008.4 | 320.0 | 0.2675 |
| GaN | 352.2 | 111.4 | 0.2687 |
| AlN | 382.5 | 130.9 | 0.2399 |
| AlAs | 1385.3 | 459.5 | 0.2518 |

The values for Poisson ratio are given only for reference. They are not directly used in our calculations.

symmetry and then repeated using the actual cubic elastic constants. For the isotropic assumption, we use the Hershey–Kröner–Eshelby method that averages the monocrystal elastic constants to provide predictions of the isotropic polycrystal. This method is known to yield the best agreement with observation and is straightforward to apply. Details are provided elsewhere [33]. These frequencies are computed for the geometries of the sphere, the paralellepiped, and the pyramid, each of which is assumed to possess identical mass. Hence the radius of the sphere, denoted as $R$, is selected as the fundamental dimension with the cube side lengths ($1.6119915R$) and the pyramid half-width and height corresponding to a height angle of $45^\circ$ (each $1.46459R$) are used in the subsequent calculations. The dimensionless frequencies shown in the results that follow are thus $\varpi = \omega R/C_t$ as was used in the initial pyramid geometry comparisons.

The resulting frequency spectra are shown in Tables 5–13. Several key features are evident. First, the frequencies for the sphere are significantly (up to about 25%) higher than those for the cube, which are in turn significantly (on the order of a factor of two) higher than the frequencies of the pyramid. This feature is consistent with the principle that as the material moves away from the center of mass of the solid, the easier it is to excite specific modes of the solid. A simple way of looking at this characteristic is to consider a parallepiped. Comparing a block of material (say of relative dimensions of 1 on a side) versus a plate of identical mass (with relative dimensions of $0.01 \times 10 \times 10$) it is clear that the lowest flexural modes of the plate will be easier to excite and thus lower than the continuum modes of the cube. Returning our discussion to the three-dimensional objects, as the material moves away from the solid center of mass, the relative stiffness (i.e. the ability of the solid resist deformation into a specific shape) is reduced and the

Table 5
Frequency spectrum for Ge

| Sphere (Cub) | Sphere (Iso) | Cube (Cub) | Cube (Iso) | Pyramid (Cub) | Pyramid (Iso) |
|---|---|---|---|---|---|
| 2.0644 (2) | 2.5011 (5) | 1.7597 (2) | 1.7716 (2) | 0.7145 | 0.7241 |
| 2.0744 (3) | 2.6338 (5) | 1.9088 (3) | 2.3692 (3) | 0.8381 | 1.0396 |
| 2.4736 (2) | 3.3283 (3) | 2.1360 (3) | 2.4215 (3) | 0.9286 | 1.0459 |
| 2.6034 (3) | 3.8647 (7) | 2.3050 (3) | 2.6809 (3) | 1.1005(2) | 1.1860 (2) |
| 2.8619 (3) | 3.8962 (7) | 2.3371 (3) | 2.7561 (3) | 1.3025(2) | 1.5643 (2) |
| 3.0337 | 4.0711 | 2.5272 (3) | 2.8943 (3) | 1.4835(2) | 1.7048 (2) |
| 3.3816 (3) | 4.7381 (5) | 2.5748 (2) | 3.1719 (2) | 1.4915 | 1.7406 |
| 3.4670 (3) | 4.9747 (9) | 2.9008 (3) | 3.3891 | 1.5417 | 1.7414 |
| 3.6292 (3) | 5.0946 (9) | 3.2051 (3) | 3.4177 (3) | 1.6001 | 1.7701 |
| 3.6305 (3) | 5.7634 (3) | 3.2458 | 3.4427 (3) | 1.6483 | 1.8744 |
| 3.6578 | 5.9853 (11) | 3.3286 | 3.7180 | 1.6872 | 1.9303 |
| 3.8584 | 6.2660 (11) | 3.3849 (3) | 3.8143 (3) | 1.8777 | 2.1126 |
| 3.9004 (2) | 6.3150 (7) | 3.4252 (3) | 3.9729 (3) | 2.0340 | 2.2727 (2) |
| 4.2241 (3) | 3.4678 (3) | 3.8859 (3) | 4.4286 (3) | 2.0879 | 2.3735 |
| 4.2603 (3) | 6.9696 (13) | 3.9668 | 4.4500 (3) | 2.1066(2) | 2.4153 |
| 4.2913 | 7.1365 (5) | 4.0306 (3) | 4.4847 (3) | 2.1159 | 2.4594 |
| 4.4797 (3) | 7.4042 (13) | 4.1719 (2) | 4.5702 | 2.1765(2) | 2.4682 (2) |
| 4.4987 (2) | 7.6377 (3) | 4.1833 (3) | 4.5893 (2) | 2.2299 | 2.4789 |
| 4.5081 (2) | 7.9231 (9) | 4.2489 (2) | 4.8660 (2) | 2.2771(2) | 2.6959 (2) |
| 4.7041 (3) | 7.9341 (15) | 4.2721 (3) | 5.0412 (3) | 2.6177 | 2.7504 (2) |
| 4.7386 (3) | 8.1280 (5) | 4.5385 (3) | 5.1546 (2) | 2.6401(2) | 2.8389 |
| 4.9916 | 8.4620 (7) | 4.5395 (2) | 5.2074 (3) | 2.6648 | 2.9729 |
| 5.1192 (3) | 5.5751 (15) | 4.6177 (3) | 5.2429 (3) | 2.7211 | 3.0392 |
| 5.2002 (3) | 9.1396 (3) | 4.6305 (2) | 5.4276 (2) | 2.8146 | 3.1717 |
| 5.2411 (3) | 9.3774 (6) | 4.7255 (3) | 5.4649 | 2.8714(2) | 3.1924 |
| 5.3510 (2) | 9.5127 (11) | 4.9426 | 5.5109 (3) | 2.9294 | 3.2219 (2) |
| 5.4197 (3) | 9.5595 (4) | 5.0300 (3) | 5.5126 (3) | 2.9868 | 3.3701 |
| 5.4664 (3) | | 5.0819 (3) | 5.5814 (3) | 3.0153 | 3.4742 |
| 5.5523 (2) | | 5.1031 (3) | 5.6025 (3) | 3.0457(2) | 3.5093 (2) |
| 5.6234 (3) | | 5.1918 (3) | 5.7793 (3) | 3.1083(2) | 3.5765 |

Table 6
Frequency spectrum for Si

| Sphere (Cub) | Sphere (Iso) | Cube (Cub) | Cube (Iso) | Pyramid (Cub) | Pyramid (Iso) |
|---|---|---|---|---|---|
| 2.1270(3) | 2.5011 (5) | 1.7616 (2) | 1.7716 (2) | 0.7169 | 0.7250 |
| 2.1290 (2) | 2.6360 (5) | 1.9646 (3) | 2.3722 (3) | 0.8614 | 1.0398 |
| 2.4778 (2) | 3.3636 (3) | 2.2040 (3) | 2.4224 (3) | 0.9519 | 1.0555 |
| 2.6107 (3) | 3.8647 (7) | 2.3583 (3) | 2.7075 (3) | 1.1134(2) | 1.1895 (2) |
| 2.9516 (3) | 3.9037 (7) | 2.3756 (3) | 2.7561 (3) | 1.3389(2) | 1.5709 (2) |
| 3.1263 | 4.1953 | 2.5693 (3) | 2.9081 (3) | 1.5165(2) | 1.7108 (2) |
| 3.4391 (3) | 4.7844 (5) | 2.6658 (2) | 3.2042 (2) | 1.5407 | 1.7481 |
| 3.5255 (3) | 4.9875 (9) | 2.9656 (3) | 3.3950 | 1.5684 | 1.7503 |
| 3.6650 (3) | 5.0946 (9) | 3.2386 (3) | 3.4185 (3) | 1.6255 | 1.7702 |
| 3.6754 (3) | 5.7634 (3) | 3.3455 | 3.4541 (3) | 1.6678 | 1.8842 |
| 3.8204 | 6.0028 (11) | 3.3813 | 3.8131 | 1.7369 | 1.9341 |
| 3.8735 | 6.2660 (11) | 3.4501 (3) | 3.8202 (3) | 1.8872 | 2.1146 |
| 4.0302 (2) | 6.3659 (7) | 3.5000 (3) | 3.9862 (3) | 2.0966 | 2.2860 (2) |
| 4.3238 (3) | 6.5740 (3) | 3.9747 (3) | 4.4449 (3) | 2.1319 | 2.3782 |
| 4.3471 (3) | 6.9914 (13) | 4.0452 | 4.4576 (3) | 2.1399(2) | 2.4432 |
| 4.3841 | 7.1366 (5) | 4.1033 (3) | 4.4970 (3) | 2.1592 | 2.4618 |
| 4.5625 (3) | 7.4043 (13) | 4.2258 (3) | 4.5704 | 2.2171(2) | 2.4731 (2) |
| 4.5683 (2) | 7.6676 (3) | 4.2259 (2) | 4.6013 (2) | 2.2743 | 2.4914 |
| 4.5905 (2) | 7.9598 (15) | 4.3544 (2) | 4.8889 (2) | 2.3318(2) | 2.7036 (2) |
| 4.7680 (3) | 7.9758 (9) | 4.4081 (3) | 5.0517 (3) | 2.6587 | 2.7616 (2) |
| 4.7793 (3) | 8.2057 (5) | 4.6001 (3) | 5.1658 (2) | 2.6629(2) | 2.8537 |
| 5.0117 | 8.4621 (7) | 4.6476 (2) | 5.2194 (3) | 2.7184 | 2.9903 |
| 5.2468 (3) | 8.5751 (15) | 4.6912 (3) | 5.2688 (3) | 2.7871 | 3.0583 |
| 5.3055 (3) | 9.1396 (3) | 4.7016 (2) | 5.4286 (2) | 2.8600 | 3.1784 |
| 5.3602 (3) | 9.4057 (5) | 4.8023 (3) | 5.5116 | 2.9264(2) | 3.2061 |
| 5.4603 (2) | 9.5648 (11) | 5.0501 | 5.5126 (3) | 2.9757 | 3.2325 (2) |
| 5.4912 (3) | 9.6270 (4) | 5.1249 (3) | 5.5313 (3) | 3.0501 | 3.3861 (2) |
| 5.5576 (3) | | 5.2046 (3) | 5.6024 (3) | 3.0912 | 3.4819 |
| 5.6149 (2) | | 5.2335 (3) | 5.6207 (3) | 3.1193(2) | 3.5252 (2) |
| 5.6884 (3) | | 5.2523 (3) | 5.7926 (3) | 3.1649(2) | 3.5873 |

Table 7
Frequency spectrum for Ag

| Sphere (Cub) | Sphere (Iso) | Cube (Cub) | Cube (Iso) | Pyramid (Cub) | Pyramid (Iso) |
|---|---|---|---|---|---|
| 1.5560 (2) | 2.5011 (5) | 1.4666 (3) | 1.7720 (2) | 0.6442 | 0.7335 |
| 1.6078 (3) | 2.6537 (5) | 1.5878 (3) | 2.3960 (3) | 0.7108 | 1.0413 |
| 2.2753 | 3.6592 (3) | 1.7354 (2) | 2.4293 (3) | 0.8620 | 1.1442 |
| 2.3035 (3) | 3.8647 (7) | 1.9953 (3) | 2.7561 (3) | 1.0117(2) | 1.2183 (2) |
| 2.4140 (2) | 3.9622 (7) | 2.0266 (3) | 2.9430 (3) | 1.0589(2) | 1.6270 (2) |
| 2.5420 (3) | 5.0896 (9) | 2.1418 (2) | 3.0256 (3) | 1.1566 | 1.7664 (2) |
| 2.9486 (3) | 5.0946 (9) | 2.4256 (3) | 3.4246 (3) | 1.3131 | 1.7712 |
| 2.9640 (3) | 5.1830 (5) | 2.4624 (3) | 3.4406 | 1.3197(2) | 1.8049 |
| 3.1794 (2) | 5.7634 (3) | 2.8164 (3) | 3.5057 (2) | 1.3202 | 1.8534 |
| 3.3342 (3) | 6.1449 (11) | 2.9324 (3) | 3.5396 (3) | 1.4710 | 1.9611 |
| 3.4823 (3) | 6.1564 | 3.0162 (3) | 3.8862 (3) | 1.5780 | 1.9690 |
| 3.5218 (3) | 6.2660 (11) | 3.1758 (3) | 4.0933 (3) | 1.7260 | 2.1406 |
| 3.7391 | 6.7978 (7) | 3.2662 | 4.5266 (3) | 1.7510 | 2.4147 |
| 3.7547 (2) | 7.1366 (5) | 3.3279 | 4.5726 | 1.7991 | 2.4237 (2) |
| 3.7984 (3) | 7.1703 (13) | 3.3496 (3) | 4.5738 (3) | 1.8059(2) | 2.4818 |
| 3.9124 | 7.3246 (3) | 3.3763 (2) | 4.5938 (3) | 1.8659 | 2.5188 (2) |
| 3.9316 (3) | 7.4043 (13) | 3.4851 | 4.7147 (2) | 1.9204(2) | 2.6062 |
| 4.2037 (3) | 8.1731 (15) | 3.6725 (3) | 4.7731 | 2.0450 | 2.6909 |
| 4.2605 (2) | 8.4075 (9) | 3.7578 (2) | 5.0772 (2) | 2.0487(2) | 2.7652 (2) |
| 4.2947 (3) | 8.4621 (7) | 3.8242 (3) | 5.1447 (3) | 2.1753 | 2.8525 (2) |
| 4.4132 (3) | 8.5751 (15) | 3.9323 (2) | 5.2785 (2) | 2.3985 | 3.0086 |
| 4.4498 (2) | 8.7255 (5) | 4.0369 (3) | 5.3359 (3) | 2.4261(2) | 3.1757 |
| 4.5195 | 9.1396 (3) | 4.1255 (3) | 5.4379 (2) | 2.4274 | 3.2363 |
| 4.5627 | 9.3210 (3) | 4.2050 (3) | 5.4881 (3) | 2.5097 | 3.2471 |
| 4.6770 (3) | 9.6356 (4) | 4.2826 (3) | 5.5126 (3) | 2.5682 | 3.3310 (2) |
| 4.6819 (3) | 9.6987 (15) | 4.2989 (2) | 5.6647 (3) | 2.5689(2) | 3.3327 |
| 4.7625 (3) | | 4.4445 (3) | 5.7830 (3) | 2.6256(2) | 3.5302 (2) |
| 4.9332 (3) | | 4.4472 (3) | 5.8281 (3) | 2.6800 | 3.5469 |
| 4.9645 | | 4.4554 | 5.9045 (3) | 2.6893(2) | 3.6521 |
| 5.0931 (3) | | 4.5267 (3) | 6.0889 (3) | 2.7385 | 3.6754 |

Table 8
Frequency spectrum for Au

| Sphere (Cub) | Sphere (Iso) | Cube (Cub) | Cube (Iso) | Pyramid (Cub) | Pyramid (Iso) |
|---|---|---|---|---|---|
| 1.5882 (2) | 2.5011 (5) | 1.4973 (3) | 1.7721 (2) | 0.6564 | 0.7364 |
| 1.6366 (3) | 2.6588 (5) | 1.6194 (3) | 2.4031 (3) | 0.7156 | 1.0418 |
| 2.3196 | 3.7506 (3) | 1.7378 (2) | 2.4313 (3) | 0.8965 | 1.1760 |
| 2.3653 (3) | 3.8647 (7) | 2.0538 (3) | 2.7561 (3) | 1.0267(2) | 1.2271 (2) |
| 2.4193 (2) | 3.9794 (7) | 2.0709 (3) | 3.0219 (3) | 1.0802(2) | 1.6450 (2) |
| 2.5544 (3) | 5.0946 (9) | 2.2266 (2) | 3.0639 (3) | 1.1853 | 1.7716 |
| 2.9756 (3) | 5.1203 (9) | 2.4574 (3) | 3.4265 (3) | 1.3343 | 1.7863 (2) |
| 3.0166 (3) | 5.3083 (5) | 2.4827 (3) | 3.4539 | 1.3438 | 1.8229 |
| 3.2763 (2) | 5.7634 (3) | 2.8468 (3) | 3.5622 (3) | 1.3573(2) | 1.8997 |
| 3.3750 (3) | 6.1884 (11) | 3.0063 (3) | 3.6141 (2) | 1.5063 | 1.9818 |
| 3.5705 (3) | 6.2660 (11) | 3.0969 (3) | 3.9141 (3) | 1.6062 | 1.9819 |
| 3.5958 (3) | 6.9301 (7) | 3.2390 (3) | 4.1261 (3) | 1.7616 | 2.1542 |
| 3.8009 (2) | 7.1365 (5) | 3.3089 | 4.5510 (3) | 1.7999 | 2.4255 |
| 3.8337 (3) | 7.2260 (13) | 3.3624 | 4.5734 | 1.8310 | 2.4792 (2) |
| 3.8620 | 7.3927 (3) | 3.4343 (2) | 4.6110 (3) | 1.8451(2) | 2.4886 |
| 3.9454 | 7.4042 (13) | 3.4433 (3) | 4.6226 (3) | 1.8814 | 2.5384 (2) |
| 4.0078 (3) | 7.9420 | 3.7309 | 4.7580 (2) | 1.9646(2) | 2.6477 |
| 4.2747 (3) | 8.2401 (15) | 3.7651 (3) | 5.0205 | 2.0893(2) | 2.7720 |
| 4.3457 (2) | 8.4620 (7) | 3.7965 (2) | 5.1352 (2) | 2.1080 | 2.7843 (2) |
| 4.3557 (3) | 8.5340 (9) | 3.8730 (3) | 5.1761 (3) | 2.2232 | 2.8801 (2) |
| 4.5195 (3) | 8.5751 (15) | 4.0315 (2) | 5.3247 (2) | 2.4591 | 3.0746 |
| 4.5355 (2) | 8.8164 (5) | 4.1186 (3) | 5.3794 (3) | 2.4781(2) | 3.2550 |
| 4.5688 | 9.1396 (3) | 4.1873 (3) | 5.4415 (2) | 2.4853 | 3.2558 |
| 4.6623 | 9.6985 (3) | 4.2425 (3) | 5.5126 (3) | 2.5827 | 3.3211 |
| 4.7395 (3) | 9.6986 (11) | 4.3447 (3) | 5.5515 (3) | 2.6167 | 3.3663 (2) |
| 4.7728 (3) | 9.6987 (3) | 4.3712 (2) | 5.6983 (3) | 2.6188(2) | 3.3780 |
| 4.8805 (3) | 9.7062 (5) | 4.5355 (3) | 5.8355 (3) | 2.6988(2) | 3.5680 |
| 5.0229 (3) | | 4.5474 (3) | 5.9305 (3) | 2.7466 | 3.5780 (2) |
| 5.1639 (3) | | 4.5677 | 5.9403 (3) | 2.7567(2) | 3.6674 |
| 5.2234 (3) | | 4.5963 (3) | 6.1396 (3) | 2.8044 | 3.7032 |

Table 9
Frequency spectrum for GaSb

| Sphere (Cub) | Sphere (Iso) | Cube (Cub) | Cube (Iso) | Pyramid (Cub) | Pyramid (Iso) |
|---|---|---|---|---|---|
| 1.9944 (2) | 2.5011 (5) | 1.7575 (2) | 1.7717 (2) | 0.7157 | 0.7265 |
| 2.0119 (3) | 2.6395 (5) | 1.8507 (3) | 2.3768 (3) | 0.8114 | 1.0401 |
| 2.4680 (2) | 3.4182 (3) | 2.0573 (3) | 2.4238 (3) | 0.9326 | 1.0707 |
| 2.6036 (3) | 3.8647 (7) | 2.3018 (3) | 2.7492 (3) | 1.0943(2) | 1.1949 (2) |
| 2.8250 (3) | 3.9150 (7) | 2.3091 (3) | 2.7561 (3) | 1.2762(2) | 1.5812 (2) |
| 2.9261 | 4.4124 | 2.5181 (3) | 2.9294 (3) | 1.4540 | 1.7203 (2) |
| 3.3161 (3) | 4.8568 (5) | 2.5491 (2) | 3.2554 (2) | 1.4698(2) | 1.7584 |
| 3.4822 (3) | 5.0070 (9) | 2.8410 (3) | 3.4039 | 1.5110 | 1.7660 |
| 3.5665 (3) | 5.0946 (9) | 3.1640 (3) | 3.4197 (3) | 1.5976 | 1.7704 |
| 3.6170 (3) | 5.7634 (3) | 3.3392 | 3.4712 (3) | 1.6374 | 1.8993 |
| 3.8511 (2) | 6.0296 (11) | 3.3549 (3) | 3.8301 (3) | 1.6500 | 1.9401 |
| 3.8775 | 6.2660 (11) | 3.3678 (3) | 3.9711 | 1.8803 | 2.1180 |
| 3.8831 | 6.4451 (7) | 3.3826 | 4.0064 (3) | 2.0223 | 2.3077 (2) |
| 4.1123 (3) | 6.7504 (3) | 3.8459 (3) | 4.4695 (3) | 2.0516 | 2.3852 |
| 4.1914 (3) | 7.0248 (13) | 3.8732 | 4.4698 (3) | 2.0762 | 2.4654 |
| 4.2526 | 7.1365 (5) | 4.0085 (3) | 4.5157 (3) | 2.1010(2) | 2.4809 (2) |
| 4.4092 (2) | 7.4042 (13) | 4.1147 (3) | 4.5708 | 2.1473(2) | 2.4870 |
| 4.4825 (2) | 7.7363 (3) | 4.1300 (2) | 4.6203 (2) | 2.2251 | 2.5113 |
| 4.5567 (3) | 7.9993 (15) | 4.1526 (3) | 4.9240 (2) | 2.2424(2) | 2.7152 (2) |
| 4.6272 (3) | 8.0571 (9) | 4.1559 (2) | 5.0682 (3) | 2.6135 | 2.7788 (2) |
| 4.7513 (3) | 8.3249 (5) | 4.4662 (2) | 5.1838 (2) | 2.6510(2) | 2.8778 |
| 4.9625 | 8.4621 (7) | 4.4949 (3) | 5.2387 (3) | 2.6584 | 3.0188 |
| 5.0056 (3) | 8.5751 (15) | 4.5657 (3) | 5.3094 (3) | 2.6592 | 3.0890 |
| 5.1050 (3) | 9.1396 (3) | 4.5906 (2) | 5.4302 (2) | 2.8260 | 3.1887 |
| 5.1353 (3) | 9.4490 (5) | 4.6929 (3) | 5.5126 (3) | 2.8453(2) | 3.2278 |
| 5.2316 (2) | 9.6443 (11) | 4.9647 (3) | 5.5604 (3) | 2.9252 | 3.2493 (2) |
| 5.3694 (3) | | 4.9893 | 5.5967 | 2.9368 | 3.4113 (2) |
| 5.4577 (3) | | 5.0465 (3) | 5.6365 (3) | 2.9553 | 3.4937 |
| 5.5404 (2) | | 5.0804 (3) | 5.6495 (3) | 2.9976(2) | 3.5506 (2) |
| 5.5533 (3) | | 5.1465 (3) | 5.8131 (3) | 3.0911(2) | 3.6037 |

Table 10
Frequency spectrum for AlSb

| Sphere (Cub) | Sphere (Iso) | Cube (Cub) | Cube (Iso) | Pyramid (Cub) | Pyramid (Iso) |
|---|---|---|---|---|---|
| 1.9716 (2) | 2.5011 (5) | 1.7568 (2) | 1.7717 (2) | 0.7165 | 0.7278 |
| 1.9909 (3) | 2.6422 (5) | 1.8319 (3) | 2.3805 (3) | 0.8026 | 1.0403 |
| 2.4660 (2) | 3.4624 (3) | 2.0313 (3) | 2.4248 (3) | 0.9374 | 1.0834 |
| 2.6043 (3) | 3.8647 (7) | 2.2989 (3) | 2.7561 (3) | 1.0929(2) | 1.1992 (2) |
| 2.8151 (3) | 3.9240 (7) | 2.3082 (3) | 2.7835 (3) | 1.2688(2) | 1.5895 (2) |
| 2.8905 | 4.6164 | 2.5192 (3) | 2.9468 (3) | 1.4428 | 1.7283 (2) |
| 3.2948 (3) | 4.9159 (5) | 2.5485 (2) | 3.2981 (2) | 1.4683(2) | 1.7669 |
| 3.5016 (3) | 5.0226 (9) | 2.8218 (3) | 3.4109 | 1.5009 | 1.7706 |
| 3.5435 (3) | 5.0946 (9) | 3.1496 (3) | 3.4206 (3) | 1.5998 | 1.7796 |
| 3.6147 (3) | 5.7634 (3) | 3.3462 | 3.4847 (3) | 1.6221 | 1.9112 |
| 3.8418 (2) | 6.0511 (11) | 3.3512 (3) | 3.8388 (3) | 1.6532 | 1.9451 |
| 3.8879 | 6.2660 (11) | 3.3521 (3) | 4.0226 (3) | 1.8826 | 2.1211 |
| 4.0077 | 6.5098 (7) | 3.4664 | 4.1092 | 2.0232 | 2.3262 (2) |
| 4.0763 (3) | 6.8977 (3) | 3.8392 (2) | 4.4794 (3) | 2.0406 | 2.3908 |
| 4.1718 (3) | 7.0517 (13) | 3.8418 | 4.4896 (3) | 2.0642 | 2.4683 |
| 4.2739 | 7.1365 (5) | 4.0088 (3) | 4.5304 (3) | 2.1002(2) | 2.4873 (2) |
| 4.3758 (2) | 7.4042 (13) | 4.0628 (3) | 4.5711 | 2.1416(2) | 2.5218 |
| 4,4862 (2) | 7.8264 (3) | 4.1173 (2) | 4.6362 (2) | 2.2290 | 2.5291 |
| 4.5995 (3) | 8.0312 (15) | 4.1228 (2) | 4.9523 (2) | 2.2345(2) | 2.7245 (2) |
| 4.6010 (3) | 8.1227 (9) | 4.1441 (3) | 5.0817 (3) | 2.6172 | 2.7926 (2) |
| 4.7643 (3) | 8.4169 (5) | 4.4525 (2) | 5.1991 (2) | 2.6397 | 2.8985 |
| 4.9513 | 8.4620 (7) | 4.4831 (3) | 5.2549 (3) | 2.6576(2) | 3.0435 |
| 4.9699 (3) | 8.5751 (15) | 4.5517 (3) | 5.3426 (3) | 2.6633 | 3.1150 |
| 5.0604 (3) | 9.1396 (3) | 4.5830 (2) | 5.4315 (2) | 2.8372 | 3.1972 |
| 5.1199 (3) | 9.4837 (5) | 4.6846 (3) | 5.5126 (3) | 2.8408(2) | 3.2459 |
| 5.1935 (20 | 9.6986 (15) | 4.9472 (3) | 5.5821 (3) | 2.9229 | 3.2633 (2) |
| 5.3614 (3) | | 5.0443 | 5.6658 (3) | 2.9296 | 3.4323 (2) |
| 5.4578 (3) | | 5.0469 (3) | 5.6734 (3) | 2.9379 | 3.5034 |
| 5.5223 (3) | | 5.0758 (3) | 5.6823 | 2.9839(2) | 3.5720 (2) |
| 5.5426 (2) | | 5.1226 (3) | 5.8298 (3) | 3.0906(2) | 3.6170 |

Table 11
Frequency spectrum for GaN

| Sphere (Cub) | Sphere (Iso) | Cube (Cub) | Cube (Iso) | Pyramid (Cub) | Pyramid (Iso) |
|---|---|---|---|---|---|
| 1.7651 (2) | 2.5011 (5) | 1.6507 (3) | 1.7717 (2) | 0.7112 | 0.7278 |
| 1.8071 (3) | 2.6423 (5) | 1.7482 (2) | 2.3806 (3) | 0.7252 | 1.0403 |
| 2.4455 (2) | 3.4648 (3) | 1.8121 (3) | 2.4249 (3) | 0.8824 | 1.0840 |
| 2.5500 (3) | 3.8647 (7) | 2.1237 (3) | 2.7561 (3) | 1.0540(2) | 1.1995 (2) |
| 2.5793 (3) | 3.9245 (7) | 2.1741 (3) | 2.7854 (3) | 1.1577(2) | 1.5900 (2) |
| 2.5880 | 4.6281 | 2.3100 (2) | 2.9477 (3) | 1.2959 | 1.7287 (2) |
| 3.1110 (3) | 4.9191 (5) | 2.4633 (3) | 3.3005 (2) | 1.3774(2) | 1.7673 |
| 3.2917 (3) | 5.0234 (9) | 2.6234 (3) | 3.4112 | 1.4121 | 1.7706 |
| 3.3984 (3) | 5.0946 (9) | 3.0029 (3) | 3.4206 (3) | 1.4652 | 1.7803 |
| 3.4836 (2) | 5.7634 (3) | 3.1214 (3) | 3.4854 (3) | 1.5287 | 1.9118 |
| 3.5167 (3) | 6.0522 (11) | 3.1584 (3) | 3.8393 (3) | 1.6035 | 1.9453 |
| 3.7556 (3) | 6.2660 (11) | 3.2602 | 4.0235 (3) | 1.8633(2) | 2.1213 |
| 3.7665 | 6.5133 (7) | 3.3127 | 4.1169 | 1.8879 | 2.3272 (2) |
| 3.8699 | 6.9055 (3) | 3.5642 | 4.4799 (3) | 1.9268 | 2.3911 |
| 3.9710 (3) | 7.0531 (13) | 3.5737 (3) | 4.4906 (3) | 1.9673(2) | 2.4685 |
| 4.0738 | 7.1365 (5) | 3.6243 (3) | 4.5312 (3) | 2.0185(2) | 2.4876 (2) |
| 4.0762 (2) | 7.4042 (13) | 3.7557 (2) | 4.5711 | 2.1109(3)[a] | 2.5234 |
| 4.3006 (3) | 7.8325 (3) | 3.8078 (3) | 4.6370 (2) | 2.4107 | 2.5303 |
| 4.3182 (2) | 8.0329 (15) | 3.9436 (2) | 4.9538 (2) | 2.5039 | 2.7250 (2) |
| 4.4487 (3) | 8.1262 (9) | 3.9931 (3) | 5.0825 (3) | 2.5190 | 2.7934 (2) |
| 4.5663 (3) | 8.4216 (5) | 4.1589 (2) | 5.1999 (2) | 2.6081(2) | 2.8996 |
| 4.6727 (3) | 8.4621 (7) | 4.3056 (3) | 5.2558 (3) | 2.6667(2) | 3.0449 |
| 4.6790 (3) | 8.5751 (15) | 4.3557 (3) | 5.3443 (3) | 2.7010 | 3.1164 |
| 4.8054 | 9.1396 (3) | 4.3874 (3) | 5.4316 (2) | 2.7307 | 3.1976 |
| 4.8213 (2) | 9.4855 (6) | 4.3938 (2) | 5.5126 (3) | 2.7336 | 3.2469 |
| 4.8578 (3) | 9.6987 (15) | 4.6087 (3) | 5.5832 (3) | 2.7460(2) | 3.2641 (2) |
| 4.9970 (3) | | 4.7058 (3) | 5.6675 (3) | 2.8089 | 3.4334 (2) |
| 5.1376 | | 4.7486 (3) | 5.6747 (3) | 2.9045(2) | 3.5039 |
| 5.1933 (3) | | 4.7800 | 5.6874 | 3.0483 | 3.5732 (2) |
| 5.3802 (3) | | 4.8178 (3) | 5.8307 (3) | 3.0673(2) | 3.6177 |

[a]Of these three frequencies, there is a lower single mode (2.110881 in our calculations) and two degenerate modes (2.110888). We do not claim this level of accuracy in our model, however, and hence they appear as three identical values in this table.

Table 12
Frequency spectrum for AlN

| Sphere (Cub) | Sphere (Iso) | Cube (Cub) | Cube (Iso) | Pyramid (Cub) | Pyramid (Iso) |
|---|---|---|---|---|---|
| 1.6417 (2) | 2.5011 (5) | 1.5395 (3) | 1.7717 (2) | 0.6782 | 0.7261 |
| 1.6940 (3) | 2.6385 (5) | 1.6834 (3) | 2.3751 (3) | 0.7051 | 1.0400 |
| 2.3711 (3) | 3.4026 (3) | 1.7414 (2) | 2.4234 (3) | 0.8329 | 1.0663 |
| 2.4090 | 3.8647 (7) | 1.9775 (3) | 2.7369 (3) | 1.0227(2) | 1.1934 (2) |
| 2.4291 (2) | 3.9118 (7) | 2.0833 (3) | 2.7556 (3) | 1.0879(2) | 1.5783 (2) |
| 2.5534 (3) | 4.3471 | 2.1383 (2) | 2.9230 (3) | 1.2031 | 1.7176 (2) |
| 3.0042 (3) | 4.8361 (5) | 2.4314 (3) | 3.2400 (2) | 1.3074(2) | 1.7555 |
| 3.1057 (3) | 5.0015 (9) | 2.5050 (3) | 3.4013 | 1.3582 | 1.7614 |
| 3.2356 (2) | 5.0946 (9) | 2.8980 (3) | 3.4192 (3) | 1.3678 | 1.7704 |
| 3.2680 (3) | 5.7634 (3) | 2.9571 (3) | 3.4659 (3) | 1.4678 | 1.8950 |
| 3.4305 (3) | 6.0221 (11) | 2.9994 | 3.8269 (3) | 1.5590 | 1.9384 |
| 3.4608 | 6.2660 (11) | 3.0037 (3) | 3.9240 | 1.7536 | 2.1170 |
| 3.5667 (3) | 6.4225 (7) | 3.2666 | 4.0002 (3) | 1.7812 | 2.3014 (2) |
| 3.8333 | 6.6990 (3) | 3.3670 (3) | 4.4624 (3) | 1.8351 | 2.3833 |
| 3.8389 | 7.0153 (13) | 3.3698 (3) | 4.4659 (3) | 1.8416 | 2.4644 |
| 3.8603 (3) | 7.1366 (5) | 3.3943 | 4.5100 (3) | 1.8591(2) | 2.4745 |
| 3.8920 (2) | 7.4042 (13) | 3.5306 (2) | 4.5703 | 1.9288(2) | 2.4786 (2) |
| 4.0716 (3) | 7.7131 (3) | 3.6421 (3) | 4.6144 (2) | 2.0089 | 2.5055 |
| 4.1710 (2) | 7.9881 (15) | 3.8274 (2) | 4.9136 (2) | 2.0369(2) | 2.7120 (2) |
| 4.2559 (3) | 8.0339 (9) | 3.8779 (3) | 5.0630 (3) | 2.2601 | 2.7740 (2) |
| 4.3201 (3) | 8.2914 (5) | 3.9473 (2) | 5.1781 (2) | 2.4013 | 2.8708 |
| 4.4405 (3) | 8.4621 (7) | 4.1296 (3) | 5.2326 (3) | 2.4117 | 3.0105 |
| 4.5727 (2) | 8.5751 (15) | 4.1746 (3) | 5.2973 (3) | 2.5002(2) | 3.0801 |
| 4.5854 (3) | 9.1396 (3) | 4.2424 (3) | 5.4291 (2) | 2.5438 | 3.1858 |
| 4.6600 | 9.4367 (5) | 4.2558 (2) | 5.5115 (3) | 2.5719(2) | 3.2216 |
| 4.6916 (3) | 9.6219 (11) | 4.4213 (3) | 5.5522 (3) | 2.6040(2) | 3.2445 (2) |
| 4.7421 (3) | | 4.4393 (3) | 5.5700 | 2.6076 | 3.4041 (2) |
| 4.7862 | | 4.4955 (3) | 5.6261 (3) | 2.6332 | 3.4903 |
| 4.9746 (3) | | 4.5134 | 5.6408 (3) | 2.7042 | 3.5432 (2) |
| 5.1511 (3) | | 4.5638 | 5.8069 (3) | 2.7415(2) | 3.5991 |

frequencies are decreased. The sphere is representative of locating the material as close to the center of mass as possible, resulting in both higher frequencies and the huge number of degenerate frequencies as shown in Tables 5–13 and Table 1.

Also of note is the change in frequency spectra when invoking assumptions of material isotropy. For each geometric shape, this assumption leads to frequencies that are significantly above those of the frequencies calculated using the cubic material elastic constants. One reason for this is the very large number of degenerate frequencies that exist for both the isotropic sphere and cube. For the pyramid, repeated frequencies are far less common, and the isotropic material assumption results in an increase of relative stiffness. To determine a bulk estimate of the influence of cubic versus isotropic material properties, the average percent relative error was calculated for the first five frequency values for each material and plotted against the degree of anisotropy $A$ introduced in Tables 3 and 4. This plot is shown in Fig. 2, and shows that there is an approximately linear change in error with change in material anisotropy.

The results presented here provide several guidelines when incorporating simplifying assumptions involving material shape and symmetry. For instance, the vast majority of past studies of quantum dot nanostructures have invoked assumptions of both spherical shape and material isotropy. The reasons for this are pragmatic. The analytical solution techniques used to study the dynamic behavior are fairly easily solved for these two conditions, including the presence of a surrounding matrix material. These past models have provided much important information regarding the physical characteristics of embedded and free-standing quantum dots. Yet the quantitative nature of these studies must be applied with caution.

Table 13
Frequency spectrum for AlAs

| Sphere (Cub) | Sphere (Iso) | Cube (Cub) | Cube (Iso) | Pyramid (Cub) | Pyramid (Iso) |
|---|---|---|---|---|---|
| 2.1544 (3) | 2.5011 (5) | 1.7625 (2) | 1.7717 | 0.7196 | 0.7268 |
| 2.1652 (2) | 2.6401 (5) | 1.9967 (3) | 2.3777 (3) | 0.8739 | 1.0401 |
| 2.4799 (2) | 3.4285 (3) | 2.2400 (3) | 2.4240 (3) | 0.9758 | 1.0736 |
| 2.6175 (3) | 3.8647 (7) | 2.3681 (3) | 2.7561 (3) | 1.1237(2) | 1.1959 (2) |
| 3.0284 (3) | 3.9172 (7) | 2.4438 (3) | 2.7572 (3) | 1.3647(2) | 1.5831 (2) |
| 3.1753 | 4.4576 | 2.6070 (3) | 2.9335 (3) | 1.5426(2) | 1.7222 (2) |
| 3.4694 (3) | 4.8706 (5) | 2.7467 (2) | 3.2653 (2) | 1.5749 | 1.7604 |
| 3.5794 (3) | 5.0107 (9) | 3.0070 (3) | 3.4055 | 1.5826 | 1.7691 |
| 3.6926 (3) | 5.0946 (9) | 3.2557 (3) | 3.4199 (3) | 1.6499 | 1.7705 |
| 3.6969 (3) | 5.7634 (3) | 3.3636 | 3.4744 (3) | 1.6869 | 1.9021 |
| 3.8928 | 6.0347 (11) | 3.4991 (3) | 3.8321 (3) | 1.7662 | 1.9413 |
| 4.0807 | 6.2660 (11) | 3.5496 (3) | 4.0027 | 1.8966 | 2.1187 |
| 4.1403 (2) | 6.4603 (7) | 3.5711 | 4.0102 (3) | 2.1552 | 2.3119 (2) |
| 4.3769 (3) | 6.7849 (3) | 4.0434 (3) | 4.4718 (3) | 2.1606 | 2.3865 |
| 4.4055 (3) | 7.0311 (13) | 4.0858 | 4.4744 (3) | 2.1728(2) | 2.4661 |
| 4.4552 | 7.1366 (5) | 4.1622 (3) | 4.5191 (3) | 2.1853 | 2.4823 (2) |
| 4.6257 (2) | 7.4043 (13) | 4.2556 (3) | 4.5708 | 2.2442(2) | 2.4953 |
| 4.6328 (2) | 7.7538 (3) | 4.2643 (2) | 4.6239 (2) | 2.3146 | 2.5152 |
| 4.6672 (3) | 8.0068 (15) | 4.4268 (2) | 4.9306 (2) | 2.3707(2) | 2.7174 (2) |
| 4.7999 (3) | 8.0724 (9) | 4.4802 (3) | 5.0713 (3) | 2.6875(2) | 2.7821 (2) |
| 4.8215 (3) | 8.3469 (5) | 4.6437 (3) | 5.1873 (2) | 2.6981 | 2.8825 |
| 5.0210 | 8.4621 (7) | 4.7181 (2) | 5.2424 (3) | 2.7693 | 3.0245 |
| 5.3289 (3) | 8.5751 (15) | 4.7443 (3) | 5.3172 (3) | 2.8280 | 3.0949 |
| 5.3815 (3) | 9.1396 (3) | 4.7531 (2) | 5.4305 (2) | 2.9087 | 3.1906 |
| 5.4233 (3) | 9.4571 (5) | 4.8686 (3) | 5.5126 (3) | 2.9692(2) | 3.2320 |
| 5.5090 (3) | 9.6592 (11) | 5.1807 | 5.5656 (3) | 3.0183 | 3.2526 (2) |
| 5.5192 (2) | | 5.1957 (3) | 5.6151 | 3.0924 | 3.4162 (2) |
| 5.6649 (3) | | 5.2798 (3) | 5.6432 (3) | 3.1420 | 3.4960 |
| 5.6693 (2) | | 5.3147 (3) | 5.6551 (3) | 3.1756(2) | 3.5510 (2) |
| 5.7605 (3) | | 5.3587 (3) | 5.8170 (3) | 3.2122(2) | 3.6068 |

The results of the present study indicate that the true physical problem for free-standing particles (i.e. the pyramid structure with cubic material symmetry) possess vibrational spectra dramatically different than those of an isotropic sphere. Although these simplifying assumptions are useful, the significant differences in quantitative response for the free-standing particles suggest that inclusion of actual physical geometry and material stiffnesses must be modeled for an accurate representation of frequency spectra.

## 4. Summary and conclusions

The acoustic spectra of free-standing particles were calculated using an approximate Ritz model. The physical representations of the dots as spheres, cubes, and pyramids with both cubic and isotropic material symmetry. Our results indicate that for particles of equal mass composed of Ge, Si, Ag, Au, GaSb, AlSb, GaN, AlN, and AlAs:

1. Frequencies for sphere geometries are up to 25% higher than those for cube geometries and about 3–4 times higher than those of pyramids.
2. The large number of degenerate frequencies for the sphere and cube geometries lead to a general increase in frequency when the assumption of isotropic material symmetry is invoked.
3. For pyramid geometries, the assumption of material isotropy as computed by effective polycrystalline elastic constants leads to an increase in frequency over those computed using the cubic material elastic constants. For the lowest five frequencies, this increase varies approximately linearly with the degree of material anisotropy.

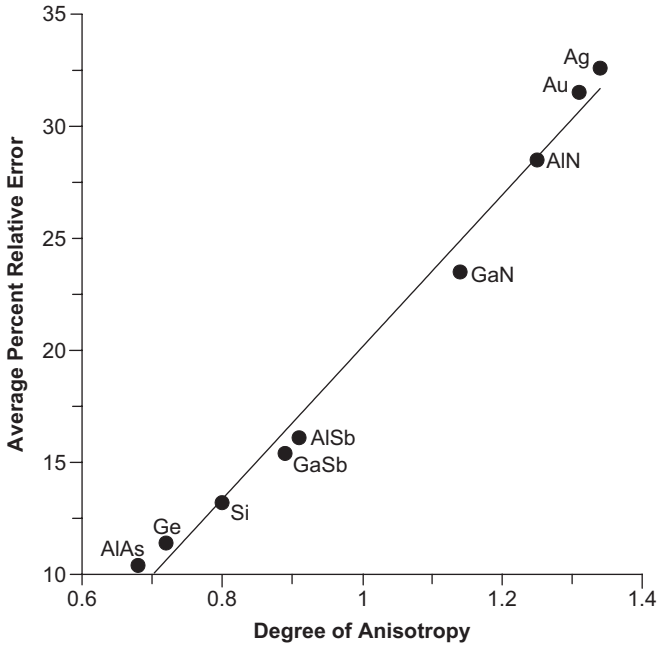


Fig. 2. Average error measures from an assumption of material isotropy as a function of the level of anisotropy for pyramids with cubic material symmetry.

In addition to these conclusions, the model used for the traction-free vibration of pyramids provide what are believed to be among the first published results of the vibrational response of free-standing pyramids. Our results compare quite favorably with those computed using a three-dimensional finite element model, and give more accurate results for a given number of degrees of freedom. The results presented in this work can be scaled to apply to structures with any dimension for purposes of comparison, but reductions to the nanoscale may be restricted by limitations of continuum theory.

## Acknowledgments

The authors would like to thank the reviewers for their constructive comments. The first author (PRH) gratefully acknowledges the support of the National Science Foundation (CMS-0301048). The second author (EP) was partially supported by ARO and AFOSR (FA9550-06-1-0317). The third (SC) and fourth (MM) authors were sponsored by the National Science Foundation (EEC-0241979).

## References

[1] J. Singh, *Physics of Semiconductors and their Heterostructures*, McGraw-Hill, Inc., New York, 1993.
[2] J.H. Davies, *The Physics of Low-Dimensional Semiconductors: an Introduction*, Cambridge University Press, Cambridge, 1998.
[3] D. Bimberg, M. Grundmann, N.N. Ledentsov, *Quantum Dot Heterostructures*, Wiley, Chichester, 1999.
[4] S. Rufo, M. Dutta, M.A. Stroscio, Acoustic modes in free and embedded quantum dots, *Journal of Applied Physics* 93 (2003) 2900–2905.
[5] F. Glas, Elastic relaxation of truncated pyramidal quantum dots and quantum wires in a half-space: an analytical calculation, *Journal of Applied Physics* 90 (2001) 3232–3241.
[6] E. Pan, Elastic and piezoelectric fields in substrates GaAs (0 0 1) and GaAs (1 1 1) due to a buried quantum dot, *Journal of Applied Physics* 91 (2002) 6379–6387.
[7] A. Tamura, K. Higeta, T. Ichinokawa, Lattice vibrations and specific heat of a small particle, *Journal of Physics C: Solid State Physics* 15 (1982) 4975–4991.
[8] A. Tanaka, S. Onari, T. Arai, Low-frequency Raman scattering from CdS microcrystals embedded in a germanium dioxide glass matrix, *Physical Review B* 47 (1993) 1237–1243.

[9] N.N. Ovsyuk, V.N. Novikov, Influence of a glass matrix on acoustic phonons confined in microcrystals, *Physical Review B* 53 (1996) 3113–3118.
[10] U. Woggon, F. Gindele, O. Wind, C. Klingshirn, Exchange interaction and phonon confinement in CdSe quantum dots, *Physical Review B* 54 (1996) 1506–1509.
[11] P.A. Knipp, T.L. Reinecke, Coupling between electrons and acoustic phonons in semiconductor nanostructures, *Physical Review B* 52 (1995) 5923–5928.
[12] A.M. Alcalde, G.E. Marques, G. Weber, T.L. Reinecke, Electron-acoustic-phonon scattering rates in II–VI quantum dots: contribution of the macroscopic deformation potential, *Solid State Communications* 116 (2000) 247–252.
[13] N.A. Fleck, On the cold compaction of powders, *Journal of the Mechanics and Physics of Solids* 43 (1995) 1409–1431.
[14] P.R. Heyliger, R.M. McMeeking, Cold plastic compaction of powders by a network model, *Journal of the Mechanics and Physics of Solids* 49 (2001) 2031–2054.
[15] C.L. Martin, D. Bouvard, S. Shima, Study of particle rearrangement during powder compaction by the discrete element method, *Journal of the Mechanics and Physics of Solids* 51 (2003) 667–693.
[16] C.L. Martin, D. Bouvard, Study of the cold compaction of composite powders by the discrete element method, *Acta Materialia* 51 (2003) 373–386.
[17] O. Skrinjar, P.-L. Larsson, On discrete element modeling of compaction of powders with size ratio, *Computational Materials Science* 31 (2004) 131–146.
[18] O. Skrinjar, P.-L. Larsson, Cold compaction of powders with size ratio, *Acta Materialia* 52 (2004) 1871–1884.
[19] P.R. Heyliger, Ritz finite elements for curvilinear particles, *Communications in Numerical Methods in Engineering* 22 (2006) 335–345.
[20] Y.C. Fung, *Foundations of Solid Mechanics*, Prentice-Hall, Englewood Cliffs, New Jersey, 1965.
[21] H. Lamb, On the vibrations of an elastic sphere, *Proceedings of the London Mathematical Society* 13 (1882) 189–212.
[22] Y. Sato, T. Usami, Basic study on the oscillation of a homogeneous elastic sphere: Part I, frequency of the free oscillations, *Geophysical Magazine* 31 (1962) 15–24.
[23] Y. Sato, T. Usami, Basic study on the oscillation of a homogeneous elastic sphere: Part II, distribution of displacement, *Geophysical Magazine* 31 (1962) 15–24.
[24] W.M. Visscher, A. Migliori, T.M. Bell, R.A. Reinert, On the normal modes of free vibration of inhomogeneous and anisotropic elastic objects, *Journal of the Acoustical Society of America* 90 (1991) 2154–2162.
[25] P.R. Heyliger, A. Jilani, The free vibrations of inhomogeneous elastic cylinders and spheres, *International Journal of Solids and Structures* 29 (1992) 2689–2708.
[26] I. Ohno, Free vibration of a rectangular parallelepiped crystal and its application to determination of elastic constants of orthorhombic crystals, *Journal of the Physics of the Earth* 24 (1976) 355–379.
[27] E. Mochizuki, Sphere-resonance method to determine elastic constants of crystal, *Journal of Applied Physics* 63 (1988) 5668–5673.
[28] W.L. Johnson, P.R. Heyliger, Symmetrization of Ritz approximation functions for vibrational analysis of cylinders, *Journal of the Acoustical Society of America* 113 (2003) 1826–1832.
[29] H.H. Demarest, Cube resonance method to determine the elastic constants of solids, *Journal of the Acoustical Society of America* 49 (1971) 768–775.
[30] P.R. Heyliger, J. Kienholz, The mechanics of pyramids, *International Journal of Solids and Structures* 43 (2006) 2693–2709.
[31] J.P. Hirth, J. Lothe, *Theory of Dislocations*, McGraw-Hill Book Company, New York, 1968.
[32] I. Vurgaftman, J.R. Meyer, L.R. Ram-Mohan, Band parameters for III–V compound semiconductors and their alloys, *Journal of Applied Physics* 89 (2001) 5815–5875.
[33] H. Ledbetter, Monocrystal-polycrystal elastic constants of stainless steels, in: M. Levy, H. Bass, R. Stern (Eds.), *Handbook of Elastic Properties of Solids, Liquids, and Gases*, Vol. II, Academic Press, St. Louis, 2000, pp. 291–297.